J Fail. Anal. and Preven. (2012) 12:267–272
DOI 10.1007/s11668-012-9555-3

TECHNICAL ARTICLE—PEER-REVIEWED

Impact Simulation on Ductile Metal Pipe with Polymer Coating by a Coupled Finite Element and Meshfree Method

Yi Gong · Zhen-Guo Yang · Yu-Fei Wang

Submitted: 12 September 2011 / in revised form: 4 January 2012 / Published online: 13 March 2012

Abstract It is common knowledge that conventional finite element method (FEM) has intrinsic limitations in analyzing large deformation problems like high-velocity impact, explosion, etc. because of mesh distortion and tangling; while these problems can be easily avoided by the meshfree method (MM), the latter involves greater computation time. Therefore, in this article, in order to simultaneously utilize the respective advantages of the two methods, a coupled simulation method between both FEM and MM was employed to analyze the high-velocity impact on ductile metal pipe with polymer coating. The impacted area with large deformation was discretized by SPH (smoothed particle hydrodynamics) particles, a classic meshfree model, and the remaining section was modeled by FEM meshes. By this method, the interfacial shear stresses between the coating and the substrate and the residual stresses beneath the contact points were studied, which would have referenced values in analyzing failure modes of components with similar composite structure. Then, the results were compared with sole FEM and MM too.

Keywords Finite element · Meshfree · Smoothed particle hydrodynamics (SPH) · Impact

Introduction

Impact, the dynamic process that hits targets with great force and causes degradation on their surfaces, is a common action on pipes with applications in fluid delivery and heat exchange in petrochemical and power generation industries [1, 2]. Its effect, particularly on the pipes in the familiar form of metal substrate and with polymer coating for, respectively, imparting structural strength and corrosion resistance, deserves to be studied in-depth for prevention of failures like erosion damage [3], and even separation between two such parts. In general, research studies on impact behavior on materials involve two types of methods: experiments and numerical simulations. In terms of the former one, a wealth of analytic models and relevant prediction equations has been obtained and reported, but most of them have limited applications since they are not able to cover all kinds of target materials, e.g., ductile or brittle [4, 5], with or without coatings [6]. As for the latter one, besides the common superiorities like cost-, effort-, and time-saving properties, finer meshes and less computation times can be usually achieved by means of the prevailing two-dimensional (2D) finite element method (FEM) [7, 8], while the 3D FEM model could even give the real weight loss of the targets and the final morphologies of their surfaces [9–12]. Nevertheless, the simplified 2D FEM model has to obey certain assumptions as plane strain, plane stress, axisymmetric, etc., and has the difficulty to solve the problem of multi-particle impact; the 3D FEM model also has its own limitations when under high-velocity impact, such as distortion of *Lagrange* meshes during large deformation, and decrease of simulation accuracy due to coarseness of the 3D grids.

In recent decades, the meshfree methods (MMs) [13], gridless models of which are discretized by a set of scattered particles rather than a series of continuous meshes, have been rapidly developed for specific applications including crack propagation [14, 15], large deformation, explosion, fluids [16], impact [17, 18], and so on, which are always encountered with mesh distortion and tangling

Y. Gong · Z.-G. Yang (✉) · Y.-F. Wang
Department of Materials Science, Fudan University, Shanghai 200433, People's Republic of China
e-mail: zgyang@fudan.edu.cn

problems in FEM. SPH (smoothed particle hydrodynamics) [19, 20], DEM (diffuse element method) [21], EFG (element-free Galerkin) [22], RKPM (reproducing kernel particle method) [23], MLSRKM (moving least-square reproducing kernel method) [24, 25], etc. are all the representative models in MMs. However, such MMs usually cost more computation times than FEM. Consequently, several algorithms coupled with both FEM and MM have been put forward to utilize the respective advantages of each of them [26–31].

In this article, a coupled simulation method between FEM and the meshfree model (MM) SPH was employed via the commercial software ANSYS/LS-DYNA to study the impact effect on ductile metal pipe with polymer coating [32]. Specifically, the impacted area (involving both the coating and the substrate) with large deformation was discretized by SPH particles while the other section with less deformation was still modeled by FEM meshes. Two different impact angles of 90° and 45° (representing the normal and the oblique impacts, respectively) were imposed, and their functions on energy evolution, plastic strain, and stresses distribution of the targets during the impact process were systematically analyzed. Finally, results of the normal impact with this coupled method were also compared with that of the sole FEM and the sole SPH method to discuss their individual advantages and disadvantages.

Modeling

The impact process was simulated by means of 3D explicit dynamic analysis in ANSYS/LS-DYNA 10.0. The *Johnson–Cook* (J–C) [33, 34] viscoplastic material model was applied for the flow stress behavior of the target materials, and the *von Mises* flow stress was accordingly expressed in Eq 1:

$$\sigma_{\mathrm{f}} = \left[A + B(\bar{\varepsilon}^{\mathrm{p}})^{n}\right]\left[1 + c\ln\left(\frac{\dot{\varepsilon}^{\mathrm{p}}}{\dot{\varepsilon}_0}\right)\right]\left[1 - \left(\frac{T - T_{\mathrm{r}}}{T_{\mathrm{m}} - T_{\mathrm{r}}}\right)^{m}\right] \quad \text{(Eq 1)}$$

where A and B are the yield stress constant and the strain hardening constant; n, c, and m are constants; $\bar{\varepsilon}^{\mathrm{p}}$ is the equivalent plastic strain; $\dot{\varepsilon}^{\mathrm{p}}$ is the plastic strain rate, and $\dot{\varepsilon}_0$ is the reference strain rate. T and T_{m} are the temperature and the melting point of the target material, while T_{r} is the room temperature. Aluminum alloy 2024-T3 Al and polyurethane (PU) were chosen as the metal substrate and the polymer coating, respectively, material constants as well as J–C parameters of which are listed in Table 1 [9, 35]. The erodent was 2 mm (diameter) aluminum spherical particle with density of 2,770 kg/m^3 and elastic modulus of 71 GPa.

In terms of the model geometry, thicknesses of the Al substrate and PU coating were 1.4 and 0.1 mm, respectively. The size of the whole target was 1.5 × 6×6 mm, as shown in Fig. 1. Specifically, the impacted area was modeled as SPH particles including 1,350 for polymer coating and 3,600 for metal substrate, and their uniform masses were, respectively, 3.733×10^{-7} and 1.385×10^{-6} kg per particle. The other section of the target was still modeled by FEM meshes with element of SOLID 164. The impact velocity was 80 m/s, and two impact angles of 90° and 45° were exerted, respectively, representing the normal and the oblique impacts. The solution time was set 1.5 × t, where t was the time that the erodent particle needed to contact the target surface.

Table 1 Material constants and Johnson-Cook parameters in the model

Materials	E, GPa	υ	A, MPa	B, MPa	n	c	m
2024-T3 Al	71	0.34	369	684	0.73	0.0083	1.7
PU coating	2.3	0.15	146	150	0.498	0.097	…

E and υ denote the elastic modulus and Poisson's ratio

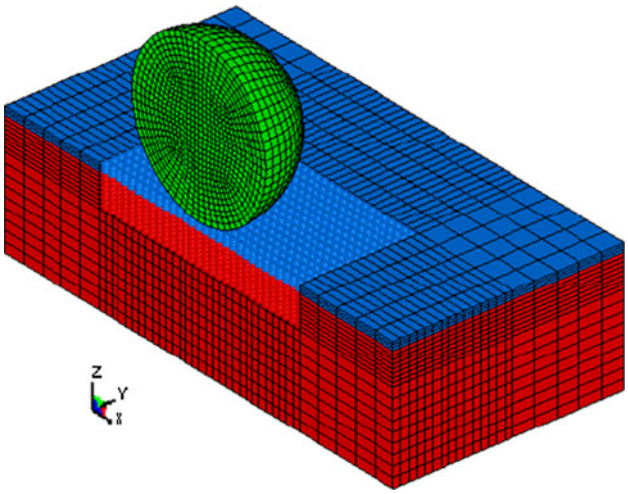

Fig. 1 Schematic diagram of the impact model

As for the constrained conditions, the tied-nodes-to-surface contact was established between the SPH scheme and the FEM meshes to couple the two sections. Besides, the eroding-nodes-to-surface contact was defined between erodent particle and the SPH section. In order to simplify the simulation, only a half-model was evaluated, and hence, the constraints and SPH symmetry planes were set for the FEM and SPH sections at the boundaries to achieve the symmetry conditions. Also, all of the bottom and outside nodes of the target materials were defined to non-reflecting boundaries.

Results and Discussion

Coupled Method

During the simulation process, the internal and the kinetic energies evolutions of the normal (90°) and the oblique

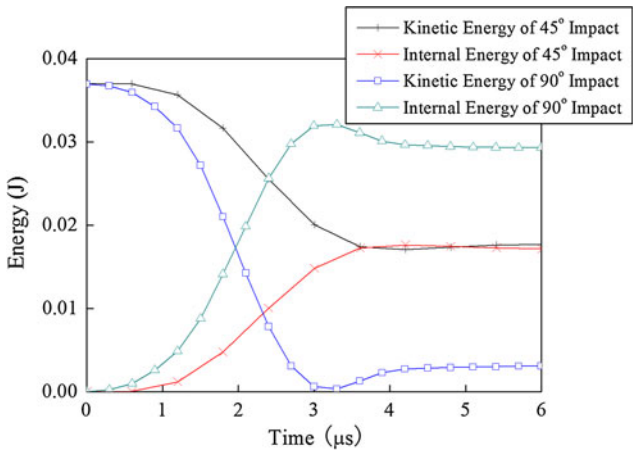

Fig. 2 Internal and kinetic energies evolutions under normal and oblique impact

(45°) impact samples are presented in Fig. 2. As shown in the curves, the initial kinetic energies of the erodent particles converted into the internal energies of the targets and the rebound kinetic energies of the particles. As for ductile target, the internal energy commonly appears in the form of plastic deformation. Thus, based on the fact as shown in Fig. 2 that the internal energy absorbed by target under 90° was higher than that under 45°, it can be concluded that greater plastic deformation was induced from normal impact than from oblique impact. This phenomenon has been verified through Fig. 3 as well: larger deformed area of the coatings after normal impact than after oblique impact.

Figure 4a and b show the interfacial shear stresses distributions between coating and substrate during impact. The shear stresses of the two samples both reached their

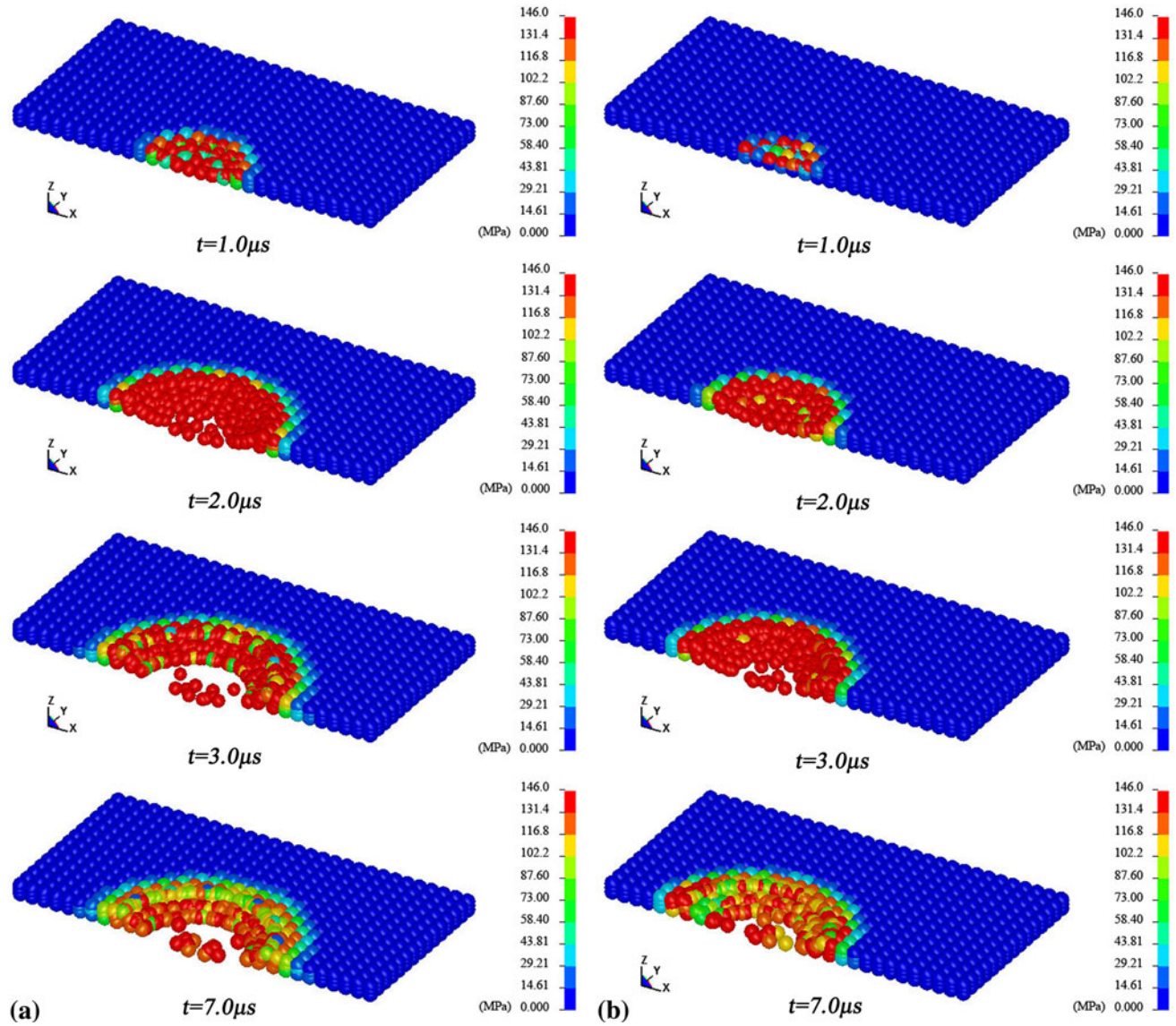

Fig. 3 Stress distribution of the coating: (**a**) normal impact; (**b**) oblique impact

maximums at 3 μs after beginning of the impact, but their locations were, respectively, about 0.3 mm (normal) and 0.2 mm (oblique) away from the contact points. This result revealed that the crater area under oblique impact was relatively smaller, testifying the phenomena in Fig. 3. However, values of these shear stresses, which were responsible for the buckling of the coating, were greater under oblique impact than those under normal impact. In other words, under oblique impact, higher possibilities would be introduced for separation between coating and substrate, and also for removal of coating material after impact.

Actually, for both normal and oblique impacts, great compressive stresses were engendered upon coatings and substrates because of erodent particles striking. Through the shot peening experiment on ductile material ANSI 4340 steel, Torres and Voorwald [36] pointed out that such compressive stress only located at limited areas on the target surface, the compressive residual stress increased below the surface until reaching a maximum depth, and then tended to decrease, transforming into the tensile residual stress. This mechanism has been verified from Fig. 5 showing that higher (compressive) residual stresses accumulated in the upper part of the metal substrate (the range from 0.1 to 0.5 mm in x-axis), and then transformed into the lower (tensile) residual stresses when the depth grew to the lower part of the substrate (the range from 0.5 to 1.5 mm in x-axis). This fact revealed that the ductile metal substrate provided adequate structural strength under impact. Meanwhile, comparatively speaking, the residual stress from normal impact (90°) was a little bit larger than that from oblique impact. This phenomenon may be attributed to the fact described as follows. As was discussed above, the greater the plastic deformation that occurred in the target under normal impact, the larger the residual stress that was left.

Comparison with FEM

In this section, results of the normal impact from the coupled method will be compared to those from the sole FEM and the sole SPH models. Table 2 tabulates the differences between the three models. Indeed, the computation time of sole FEM model was much less than those with SPH particles, and the resulting curve was even smoother, as seen in Fig. 5. However, obvious distortion occurred on the FEM meshes within the impacted area (Fig. 6a), while the crater of the SPH particles was free of this problem (Fig. 6b). This could be explained by the fact that the FEM elements were connected by nodes, and thus its result was relatively smooth but inaccurate because of element distortion under such high-velocity impact. Comprehensively speaking, the coupled method yielded reasonable results, and also involved cost-effective computation time.

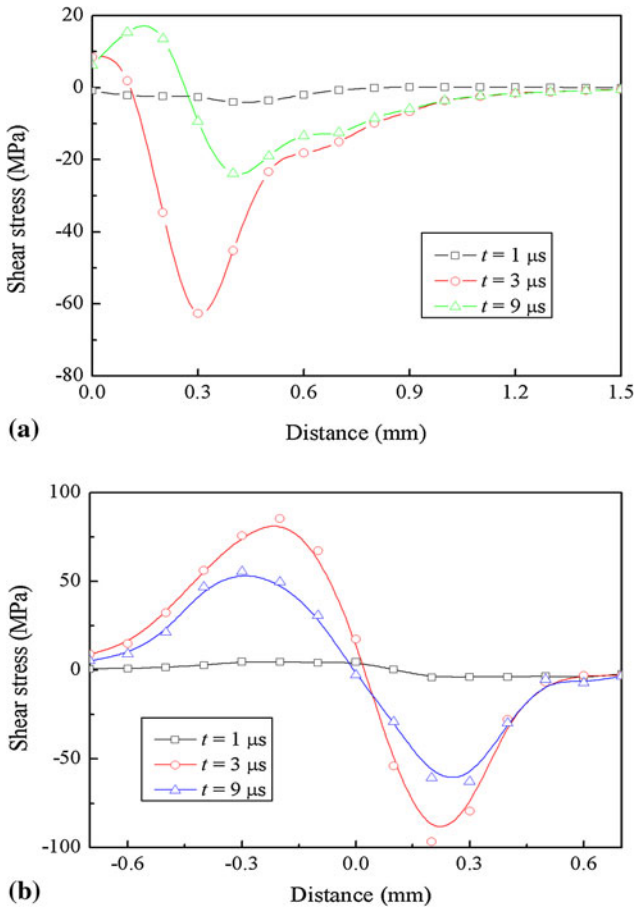

Fig. 4 Interfacial shear stresses between coating and substrate: (**a**) normal impact; (**b**) oblique impact

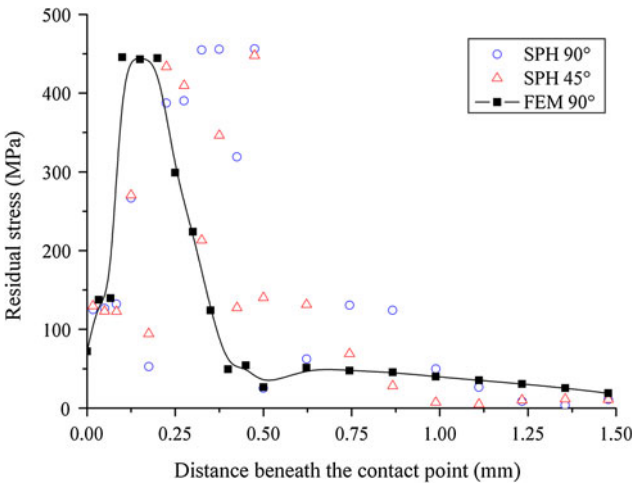

Fig. 5 Residual stresses beneath the contact points (along the path of z-axis)

Table 2 Comparison between coupled method and sole FEM, and sole SPH methods

Methods	Number of elements	Number of SPH	Results[a], MPa	CPU time, s
FEM model	24,192	…	340	242
Sole SPH model	…	24,192	354	2,334
Coupled model	19,242	4,950	352	836

[a] The results in MPa are the equivalent stresses of the node at the impact point under normal impact

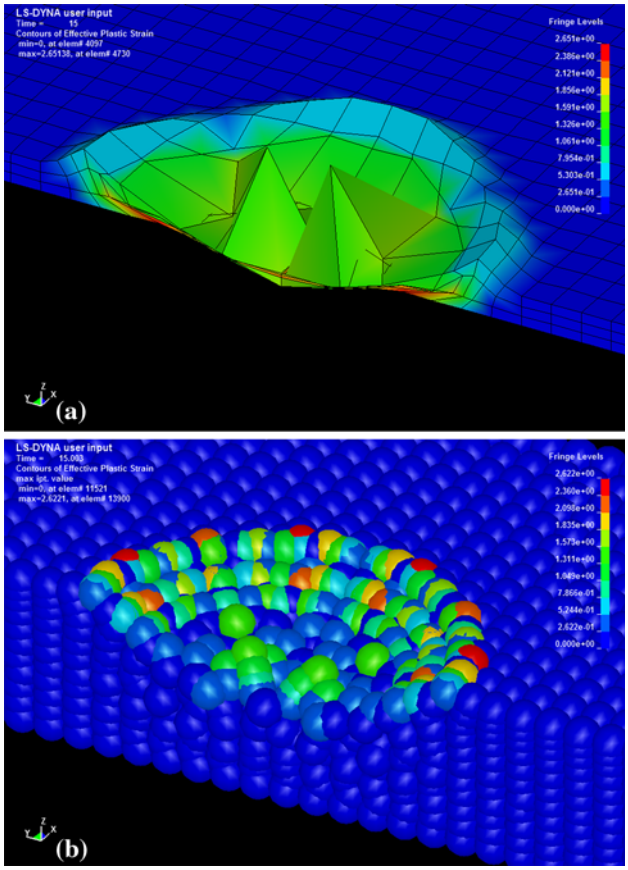

Fig. 6 Plastic strain of the impacted area: (**a**) from FEM; (**b**) from coupled method (sole SPH method was same)

Conclusions

(1) A coupled model with both FEM and MM was utilized to analyze the high-velocity impact on metal substrate pipe with polymer coating, effectively avoiding the mesh distortion and tangling problems in sole FEM simulation.

(2) Two impact angles of 90° and 45° were, respectively, applied via this coupled model to compare their influences on energy evolutions, surface morphologic transformations, and shear and residual stresses distributions.

Acknowledgments This study was supported by the Shanghai Leading Academic Discipline Project (Project Number: B113). Meanwhile, Yi Gong also appreciate the help from Professor Shaofan Li's research group in Department of Civil and Environmental Engineering at University of California, Berkeley under the Short-term International Exchange Programme Fund for Doctoral Students of Fudan University.

References

1. Gong, Y., Yang, Z.G., Yuan, J.Z.: Failure analysis of leakage on titanium tubes within heat exchangers in a nuclear power plant. Part II. Mechanical degradation. Mater. Corros. **63**, 18–28 (2012)
2. Gong, Y., Zhong, J., Yang, Z.G.: Failure analysis of bursting on the inner pipe of a jacketed pipe in a tubular heat exchanger. Mater. Des. **31**, 4258–4268 (2010)
3. Wood, R.J.K.: The sand erosion performance of coatings. Mater. Des. **20**, 179–191 (1999)
4. Hutchings, I.M.: Particle erosion of ductile metals: a mechanism of material removal. Wear **27**, 121–128 (1974)
5. Hutchings, I.M.: Ductile-brittle transitions and wear maps for the erosion and abrasion of brittle materials. J. Phys. D Appl. Phys. **25**, A212–A221 (1992)
6. Barkoula, N.M., Karger-Kocsis, J.: Review processes and influencing parameters of the solid particle erosion of polymers and their composites. J. Mater. Sci. **37**, 3807–3820 (2002)
7. Shimizu, K., et al.: FEM analysis of the dependency on impact angle during erosive wear. Wear **233–235**, 157–159 (1999)
8. Chen, Q., Li, D.Y.: Computer simulation of solid particle erosion. Wear **254**, 203–210 (2003)
9. Zouari, B., Touratier, M.: Simulation of organic coating removal by particle impact. Wear **253**, 488–497 (2002)
10. Har, J., Fulton, R.E.: A parallel finite element procedure for contact-impact problems. Eng. Comput. **19**, 67–84 (2003)
11. Griffin, D., Daadbin, A., Datta, S.: The development of a three-dimensional finite element model for solid particle erosion on an alumina scale/MA956 substrate. Wear **256**, 900–906 (2004)
12. Aquaro, D.: Erosion due to the impact of solid particles of materials resistant at high temperature. Meccanica **41**, 539–551 (2006)
13. Nguyen, V.P., Rabczuk, T., Bordas, S., Duflot, M.: Meshless methods: a review and computer implementation aspects. Math. Comput. Simulat. **79**, 763–813 (2008)
14. Rabczuk, T., Belytschko, T.: Cracking particles: a simplified meshfree method for arbitrary evolving cracks. Int. J. Numer. Methods Eng. **61**, 2316–2343 (2004)
15. Rabczuk, T., Belytschko, T.: A three-dimensional large deformation meshfree method for arbitrary evolving cracks. Comput. Method Appl. M **196**, 2777–2799 (2007)
16. Rabczuk, T., Gracie, R., Song, J.H., Belytschko, T.: Immersed particle method for fluid–structure interaction. Int. J. Numer. Methods Eng. **81**, 48–71 (2010)
17. Zeng, X.W., Li, S.F.: A multiscale cohesive zone model and simulations of fracture. Comput. Methods Appl. Mech. Eng. **199**, 547–556 (2010)

18. Ren, B., Li, S.F.: Meshfree simulations of plugging failures in high-speed impacts. Comput. Struct. **88**, 909–923 (2010)
19. Lucy, L.B.: A numerical approach to the testing of the fission hypothesis. Astron. J. **8**, 1013–1024 (1977)
20. Gingold, R.A., Monaghan, J.J.: Smoothed particle hydrodynamics: theory and application to non-spherical stars. Mon. Not. R. Astr. Soc. **181**, 375–389 (1977)
21. Nayroles, B., Touzot, G., Villon, P.: Generalizing the elements. Comput. Mech. **10**, 307–318 (1992)
22. Belytschko, T., Lu, Y.Y., Gu, L.: Element-free Galerkin methods. Int. J. Numer. Methods Eng. **37**, 229–256 (1994)
23. Liu, W.K., Jun, S., Zhang, Y.F.: Reproducing kernel particle methods. Int. J. Numer. Methods Fluids **20**, 1081–1106 (1995)
24. Liu, W.K., Li, S.F., Belytschko, T.: Moving least-square reproducing kernel methods (I). Methodology and convergence. Comput. Method Appl. M **143**, 113–154 (1997)
25. Li, S.F., Liu, W.K.: Moving least-square reproducing kernel method. Part II. Fourier analysis. Comput. Method Appl. M **139**, 159–193 (1996)
26. Huera, A., Fernandez-Mendez, S.: Enrichment and coupling of the finite element and meshless methods. Int. J. Numer. Mech. Eng. **48**, 1615–1636 (2000)
27. Wu, C.T., Botkin, M.E., Wang, H.P.: Development of a coupled finite element and mesh-free method in LS-DYNA. In: 7th International LS-DYNA Users Conference, Dearborn, Michigan, pp. 1229–1240 (2002)
28. Rabczuk, T., Xiao, S.P., Sauer, M.: Coupling of meshfree methods with finite elements: basic concepts and test results. Commun. Numer. Methods Eng. **22**, 1031–1065 (2006)
29. Wang, H.P., Wu, C.T., Guo, Y., Botkin, M.E.: A coupled meshfree/finite element method for automotive crashworthiness simulations. Int. J. Impact Eng. **36**, 1210–1222 (2009)
30. Johnson, G.R., Beissel, S.R., Gerlach, C.A.: Another approach to a hybrid particle-finite element algorithm for high-velocity impact. Int. J. Impact Eng. **38**, 397–405 (2011)
31. Wang, Y.F., Yang, Z.G.: A coupled finite element and meshfree analysis of erosive wear. Tribol. Int. **42**, 373–377 (2009)
32. Holmberg, K., Matthews, A., Ronkainen, H.: Coatings tribology-contact mechanisms and surface design. Tribol. Int. **31**, 107–120 (1998)
33. Johnson, G.R., Cook, W.H.: A constitutive model and data for metals subjected to large strains, high strain rates and high temperatures. In: Proceedings of the 7th International Symposium on Ballistics, The Hague, pp. 541–547 (1983)
34. Johnson, G.R., Cook, W.H.: Fracture characteristics of three metals subjected to various strains, strain rates, temperatures and pressures. Eng. Fract. Mech. **21**, 31–48 (1985)
35. Kay, G.: Failure Modeling of Titanium 6Al–4V and Aluminum 2024-T3 with the Johnson–Cook Material Model. Tech. Rep. DOT/FAA/AR-03/57. US Department of Transportation, Federal Aviation Administration (2003)
36. Torres, M., Voorwald, H.: An evaluation of shot peening, residual stress and stress relaxation on the fatigue life of AISI 4340 steel. Int. J. Fatigue **24**, 877–886 (2002)